Enhancement of thermovoltage and tunnel magneto-Seebeck effect in CoFeB-based magnetic tunnel junctions by variation of the MgAl2O4 and MgO barrier thickness

Huebner, Torsten; Martens, Ulrike; Walowski, Jakob; Boehnke, Alexander; Krieft, Jan; Heiliger, Christian; Thomas, Andy; Reiss, Guenter; Kuschel, Timo; Muenzenberg, Markus

Published in:
Physical Review B

DOI:
10.1103/PhysRevB.96.214435

Publication date:
2017

Enhancement of thermovoltage and tunnel magneto-Seebeck effect in CoFeB-based magnetic tunnel junctions by variation of the $MgAl_2O_4$ and MgO barrier thickness

Torsten Huebner,[1,*] Ulrike Martens,[2] Jakob Walowski,[2] Alexander Boehnke,[1] Jan Krieft,[1] Christian Heiliger,[3] Andy Thomas,[4] Günter Reiss,[1] Timo Kuschel,[1,5] and Markus Münzenberg[2]

[1]*Center for Spinelectronic Materials and Devices, Department of Physics, Bielefeld University, Universitätsstraße 25, 33615 Bielefeld, Germany*

[2]*Institut für Physik, Greifswald University, Felix-Hausdorff-Strasse 6, 17489 Greifswald, Germany*

[3]*Institut für Theoretische Physik, Justus Liebig University Giessen, Heinrich-Buff-Ring 16, 35392 Giessen, Germany*

[4]*Leibniz Institute for Solid State and Materials Research Dresden (IFW Dresden), Institute for Metallic Materials, Helmholtzstrasse 20, 01069 Dresden, Germany*

[5]*Physics of Nanodevices, Zernike Institute for Advanced Materials, University of Groningen, Nijenborgh 4, 9747 AG Groningen, The Netherlands*

(Received 22 June 2017; revised manuscript received 16 October 2017; published 26 December 2017)

We investigate the influence of the barrier thickness of $Co_{40}Fe_{40}B_{20}$-based magnetic tunnel junctions (MTJs) on the laser-induced tunnel magneto-Seebeck (TMS) effect. Varying the barrier thickness from 1 to 3 nm, we find a distinct maximum in the TMS effect for a 2.6-nm barrier thickness. This maximum is measured independently for two barrier materials, namely, $MgAl_2O_4$ (MAO) and MgO. Additionally, samples with a MAO barrier exhibit a high thermovoltage of more than 350 μV in comparison to 90 μV for the MTJs with a MgO barrier when heated with the maximum laser power of 150 mW. Our results allow for the fabrication of improved stacks when dealing with temperature differences across MTJs for future applications in spin caloritronics, the emerging research field that combines spintronics and thermoelectrics.

DOI: 10.1103/PhysRevB.96.214435

I. INTRODUCTION

In recent years, the combination of the spintronic *magnetic tunnel junction* (MTJ) and a temperature gradient were studied intensively [1–17]. Since these experiments combine spin, charge, and heat-driven currents, they are prominent examples for the emerging topic of spin caloritronics [18], which might provide a possibility to utilize the otherwise wasted heat in today's memory and sensing applications. To achieve this goal, an extensive knowledge about the involved thermal processes in nanostructures is key.

At first, the *tunnel magneto-Seebeck* (TMS) effect was predicted [1] and measured with two different techniques, laser induced [2] and extrinsically heated with a nanostructured heater line [3]. Later on, the experimentally even more challenging *tunnel magneto-Peltier effect*, which is reciprocal to the TMS effect, was observed as well [7]. Subsequent studies focused on the increase in effect sizes, film quality, and the overcoming of experimental challenges.

In particular, a giant TMS ratio of -3000% was found when applying an additional bias voltage across the MTJ [8], and a significant improvement of the TMS ratio was obtained with the usage of half-metallic electrodes from ferromagnetic Heusler compounds, such as Co_2FeAl or Co_2FeSi [9], and parasitic effects originating from semiconducting substrates were clarified [10]. Additionally, in a preceding publication [11], we compared the laser-induced TMS with the method of the intrinsic TMS, which uses a symmetry analysis of the tunneling current with respect to the applied voltage. The model of Brinkman *et al.* [19] offered an alternative way to explain the symmetric contribution previously associated with the intrinsic TMS. Thus, we concluded that it is not possible to explicitly observe an intrinsic TMS.

Up to now, theoretical works focused only on six or ten atomic layers, respectively, of barrier thickness and on the electrode/barrier interface, which hugely influences not only the tunnel magnetoresistance (TMR), but also the TMS effect [20,21]. Fe-Co/MgO is used often as a model system within these studies due to the large computational effort that is necessary, e.g., to model the TMS for materials with a more complex crystal structure. Furthermore, Fe-Co/MgO exhibits coherent tunneling of the electrons via Δ_1 states and, thus, ensures high-TMR ratios needed for applications. A combination of an additionally applied temperature gradient and the continuing improvement of Seebeck voltages and TMS ratios will support the development of green energy-efficient waste heat recovery devices. In addition, the in-depth understanding of connections among spin, charge, and heat currents in MTJs will pave the way towards related spin caloritronic effects, such as the thermal spin-transfer torque [22–26].

Previous TMS measurements concentrated on the established MTJ system of Co-Fe(CoFeB)/MgO with a standard barrier thickness of around 2 nm. Therefore, we investigate the system of CoFeB and $MgAl_2O_4$ (MAO) with different barrier thicknesses and junction sizes in order to maximize the TMS effect. Theoretically, MAO exhibits an advantageous lattice mismatch (1%) with standard ferromagnetic electrodes, such as Fe, CoFe, or CoFeB when compared to MgO [(3–5)%] [27]. As a barrier, MAO also enables coherent tunneling via the Δ_1 symmetry filter effect [28]. So far, experimental results of the TMR effect in MAO MTJs fall short in comparison to MgO MTJs [29–31], but, for example, magnetization switching by *spin-transfer torque* has been demonstrated [32]. Additionally, by growing MAO barriers via *molecular*

*thuebner@physik.uni-bielefeld.de

TABLE I. Overview of different nominal barrier thicknesses of each series.

Series	Nominal barrier thickness (nm)
I (MAO)	1.0 1.4 1.6 1.8[a] 2.0[a] 2.2 2.6 3.0
II (MgO)	1.2 1.5 1.8 1.9 2.0 2.3 2.6 2.9

[a]Samples were prepared independently of the rest of the series.

beam epitaxy, $MgAl_2O_x$ double-barrier MTJs exhibit almost no lattice mismatch between electrode and barrier showing pronounced resonant tunneling features in quantum well structures [33]. As a direct comparison with recent experiments and theoretical predictions, we compare our results for MAO barriers with CoFeB/MgO MTJs.

This paper is organized as follows: Sec. II starts with the sample deposition and preparation, followed by Sec. III, which is split into three subsections. Here, Sec. III A deals with the results of the TMR and TMS measurements, Sec. III B deals with the results of the I/V curves, and Sec. III C deals with the thermovoltage and COMSOL evaluation. Section IV concludes this paper.

II. SAMPLE DEPOSITION AND PREPARATION

We prepared different sample series in order to give a detailed overview concerning reproducibility and comparability. The MAO and MgO MTJs are sputtered in a Leybold Vakuum GmbH CLAB 600 cluster tool at a base pressure of less than 5×10^{-7} mbar. This system allows the deposition of several samples without exposing them to ambient conditions in between sputtering processes. The whole stack of all series is composed of a bottom contact of Ta 10/Ru 30/Ta 5/Ru 5, a tunnel junction of $Mn_{83}Ir_{17}$ 10/$Co_{40}Fe_{40}B_{20}$ 2.5/barrier/$Co_{40}Fe_{40}B_{20}$ 2.5, and a top contact of Ta 5/Ru 30/Ta 5/Au 60 (the numbers are nominal thicknesses in nanometers). The resulting sample series are summarized in Table I. Two samples of series I are prepared independently of the rest of the series.

To achieve the exchange biasing of the ferromagnetic electrode by MnIr, the stacks are postannealed at 350 °C for 1 h, followed by cooling in a magnetic field of 0.7 T. *Electron-beam lithography* and *ion-beam etching* are used to pattern elliptical junctions of 0.5π, 2π, and 6π μm^2 with the major axis being twice as large as the minor axis. Ta_2O_5 (120 nm) is used as insulating material between individual MTJs, and Au bond pads serve as electrical contacts and heat absorbers.

In order to measure the TMR effect and I/V characteristics, a *Keithley 2400 Sourcemeter* is used. For the generation of the thermovoltage, a modulated diode laser with a wavelength of 637 nm is focused via a confocal microscope onto the MTJ and generates a heat difference across the MTJ since the substrate of the sample acts as a heat sink. A frequency of 177 Hz, serving as a reference for the detection of the thermovoltage via a lock-in amplifier, and the maximum laser power of 150 mW is used. The size of the laser spot is freely adjustable by moving the sample in the direction of the beam, which has been studied intensively by Martens *et al.* [12]. Furthermore, a thorough description of the setup to measure laser-induced thermovoltages and TMS effects in MTJs is given by Boehnke *et al.* [10].

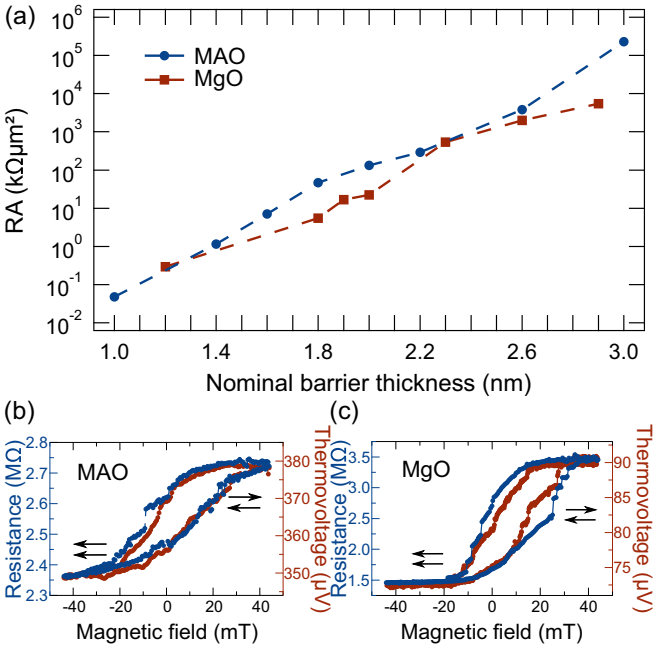

FIG. 1. (a) Averaged RA products for the MAO MTJs (the blue circles) and the MgO MTJs (the red squares) in the parallel state. (b) and (c) Exemplary minor loops with the highest switching ratios of the samples with MAO and MgO barriers, respectively. Both loops are measured at the smallest junction area of 0.5π μm^2.

III. RESULTS

A. TMR and TMS results

Figure 1(a) shows the resistance area (RA) products of both series depending on the nominal barrier thicknesses in the parallel magnetization alignment. Please note that the error bars of the RA product are too small to be seen, indicating an overall homogenous sample quality of all series. As expected, the RA product increases exponentially with increasing nominal barrier thickness. In addition, the RA products of the independently prepared samples within series I fit very well together. Thus, the independent deposition of the samples of series I allows a direct comparison of the MTJs.

Since the RA product is governed mostly by the barrier, it is noteworthy that the different barrier materials lead to comparable RA values between the series. Two minor loops of the samples with the highest TMS ratios are shown in Figs. 1(b) and 1(c). Here, the nominal barrier thickness is 2.6 nm, and the junction size is 0.5π μm^2 in both cases. Despite the high resistance resulting from the thick barrier of 2.6 nm, both MTJs show parallel and antiparallel states with the same switching behavior for TMS and TMR measurements. The extracted TMS (TMR) ratio amounts to 8% (18%) for MAO, whereas it is 28% (130%) for MgO. The sample with the MAO barrier shows a very high thermovoltage of around 375 μV in contrast to around 80 μV in the case of a MgO barrier when using a laser power of 150 mW. In addition, the minor loops presented in Figs. 1(b) and 1(c) exhibit a different squareness in contrast to samples with thinner barriers (cf. minor loops with a barrier

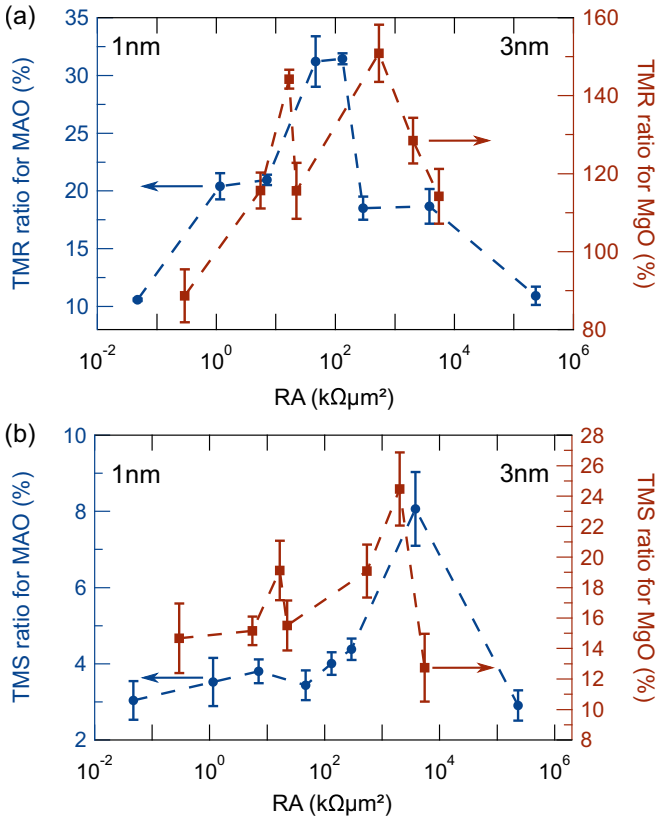

FIG. 2. (a) Averaged TMR ratios of all measured elements with resulting error bars versus RA: MAO (the left axis, blue circles) and MgO (the right axis, red squares). (b) Averaged TMS ratios of all measured elements with resulting error bars versus RA: MAO (the left axis, blue circles) and MgO (the right axis, red squares).

of 1.8-nm MAO in Ref. [11]). We attribute this difference to a change in the interlayer exchange coupling in line with results presented in Ref. [34].

Figure 2(a) summarizes the results of the TMR measurements of series I and II depending on the RA product. For each barrier thickness several elements as well as different element areas are measured and averaged. First, both barrier materials show TMR maximum values (MAO: 30%, MgO: 150%) around a nominal barrier thickness of 2 nm ($RA_{MAO} \approx 100\ k\Omega\,\mu m^2$, $RA_{MgO} \approx 1000\ k\Omega\,\mu m^2$). Second, the series with the MgO barrier exhibits a second peak of the TMR for a barrier thickness of 1.9 nm ($RA = 10\ k\Omega\,\mu m^2$). This peak might be related directly to the slightly increased RA product [cf. Fig. 1(a)] in this region.

The dependence of the TMS ratio on the barrier thickness of both series is shown in Fig. 2(b). Thin barriers of MAO exhibit a gradual increase in TMS ratios from 3% to 4%, whereas a distinct maximum is observed for a nominal barrier thickness of 2.6 nm. Here, the TMS ratio doubles to 8%. Furthermore, the TMS ratio of the MTJs with the MgO barrier shows a similar behavior. It rises from 14% to 19% in the case of thin barriers and shoots up to almost 28% for a nominal barrier thickness of 2.6 nm. In between, a local maximum is observable that directly corresponds to the position of the local TMR maximum. The errors of the TMR and the TMS ratios result from averaging over all measured elements.

Theoretically, since the TMS ratio depends on the asymmetry of the transmission function around the Fermi energy and the TMR ratio depends on the absolute number of states, a direct correlation between TMR and TMS ratios is not expected [1,21,35]. This statement is supported by the first measurements of Co_2FeSi- and Co_2FeAl-based MTJs and corresponding theoretical considerations by Boehnke *et al.* [9]. For both barrier materials, the TMS peak is located around the same value of RA of some $10^3\ k\Omega\,\mu m^2$'s, which corresponds to a nominal barrier thickness of 2.6 nm. Also, the TMS ratios of the samples prepared separately correspond well to the results of the rest of series I. Thus, we expect a similar asymmetry of the transmission function of these samples.

In contrast to our experiments, theoretical calculations predict an increasing TMS ratio when going down from ten monolayers (MLs) (2%) to six monolayers (10%) of MgO [21] (1 ML $\cong$ 2.1 Å). A reason for these opposite results might be a different interface structure of the electrode and the barrier, which is assumed to be ordered perfectly in the calculations. Czerner and Heiliger [20] find the TMS to be very sensitive to the interface termination of the magnetic material and the barrier.

B. I/V measurements

Figures 3(a) and 3(b) show the dJ/dV (recalculated from I/V measurements) curves that are measured at the same elements as in Figs. 1(b) and 1(c). Although the curves look similar in the case of a MTJ with a MAO barrier, they look very different in the case of the MTJ with the MgO barrier. This difference is due to the coherent tunneling of MgO-based MTJs: The parallel curve is almost linear, whereas the antiparallel curve exhibits a pronounced kink around a bias voltage of 0 V. Since the MAO MTJs exhibit a rather low TMR, no Δ_1 symmetry filter effect and, thus, no coherent tunneling are present in the MTJs with the MAO barrier.

In order to further analyze the MTJs with the MAO barrier, we use the model of Brinkman *et al.* [19], which allows us to calculate the barrier height φ, the barrier asymmetry $\Delta\varphi$, and the barrier thickness d_B from the I/V measurements. A theoretical description of this model can be found in Ref. [19], whereas the experimental details are described in Ref. [11]. With this model, we are able to quantitatively compare the samples with different MAO barrier thicknesses. One drawback of the Brinkman model is its limitation to MTJ systems that do not show coherent tunneling. In addition, it is not able to explain features resulting from density of states related effects, such as half-metallic ferromagnetism. Thus, it is not possible to extract physically reasonable barrier parameters of the MTJs with a MgO barrier because of the coherent tunneling resulting from the Δ_1 symmetry filter effect.

Figure 3(c) depicts the relative deviation of the calculated Brinkman barrier thickness (d_B) from the nominal barrier thickness (d_N). With respect to the error range of the Brinkman model of 10% (as stated by Brinkman *et al.* [19] in their original work, marked by the gray area), most of the elements are very close to the nominal barrier thickness. Except for the sample with a MAO barrier thickness of 1.4 nm, this deviation does not exceed 15%. An additional requirement of the Brinkman model to be applicable is $d_N > 1.0$ nm. Apparently,

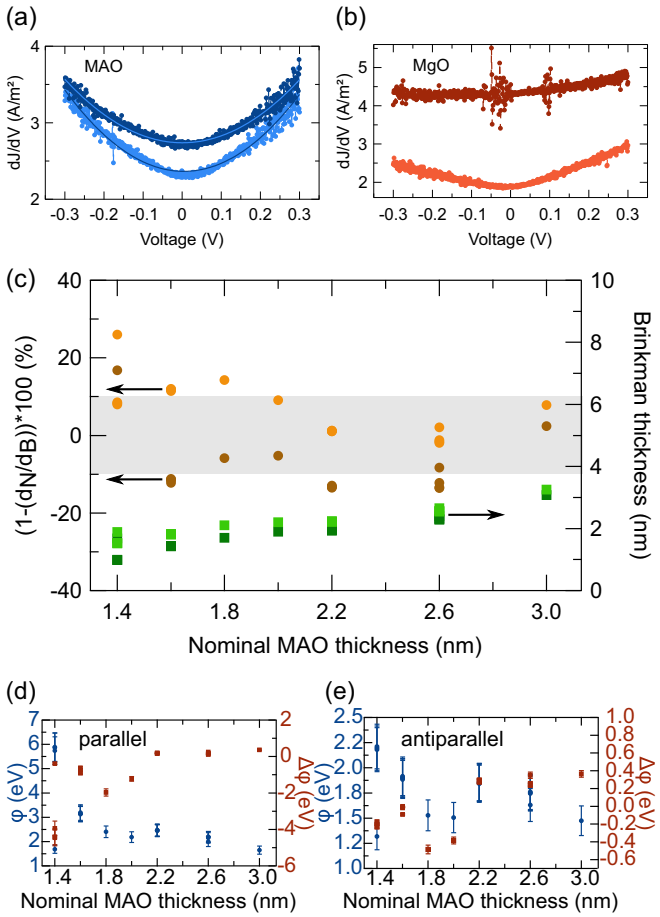

FIG. 3. (a) dJ/dV data of the MTJ with a MAO barrier (2.6 nm, 0.5π μm^2) with the Brinkman fits that are used to extract barrier parameters (dark: parallel, light: antiparallel). (b) dJ/dV data of the MTJ with a MgO barrier (2.6 nm, 0.5π μm^2) (dark: parallel, light: antiparallel). (c) Relative deviation of the nominal barrier thickness (d_N) and the calculated Brinkman barrier thickness (d_B). Dark (light) orange represents the results of the parallel (antiparallel) state. Please note that several element sizes are depicted that are partially overlapping in order to demonstrate the consistency of the method. The green squares are the extracted Brinkman thicknesses for each nominal MAO barrier thickness (dark: parallel, light: antiparallel). The gray area represents the typical error range of the Brinkman model of 10%. (d) and (e) Barrier height φ (blue circles) and asymmetry $\Delta\varphi$ (red squares) values for all measured elements and barrier thicknesses in the (d) parallel and (e) antiparallel states.

the nominal barrier thickness of 1.4 nm is too close to this limit, resulting in huge variations of the Brinkman barrier parameters. Since all other Brinkman barrier thicknesses are very close to the nominal thickness, and the RA values of the MAO- and MgO-based MTJs are also very close, we assume that the nominal barrier thicknesses of both series are close to the real thickness, which is important for future theoretical and experimental works.

In general, the calculated Brinkman barrier thicknesses depicted by the green squares in Fig. 3(c) are larger in the antiparallel (light) than in the parallel state (dark). For the barrier height and the barrier asymmetry in Figs. 3(d) and 3(e), we find a reversed behavior. Here, the parallel values [Fig. 3(d)] are generally larger than the antiparallel ones [Fig. 3(e)]. Again, the results of the sample with a barrier thickness of 1.4-nm MAO show a huge variation, whereas the results of all other samples are very consistent, even between different junction sizes. Excluding the results of the sample with a MAO barrier of 1.4 nm, the barrier height decreases from 3 to 1.7 eV (1.9 to 1.5 eV) in the parallel (antiparallel) state.

Additionally, the barrier asymmetry increases from −1 to 0.5 eV in the parallel state, whereas it increases from −0.1 to 0.4 eV in the antiparallel state. Overall, the calculated values of the samples that have been prepared independently from the rest of the series (1.8 and 2.0 nm) show almost no deviation from the general trend in the case of the barrier height. However, the values of the barrier asymmetry are different for the independently prepared samples. A possible explanation for this difference might be the deposition process, which plays a vital role for the barrier asymmetry. Nevertheless, since the TMS ratios agree very well, the geometric barrier asymmetry seems to have no significant influence on the asymmetry of the transmission function.

C. Thermovoltages and Seebeck coefficients

In order to investigate the high thermovoltages of the sample with the MAO barrier, Fig. 4(a) depicts the thermovoltage depending on the MTJ area of the sample with a nominal MAO barrier thickness of 2.6 nm. Furthermore, the remaining thermovoltage after a dielectric breakdown of the junction is shown [see the inset of Fig. 4(a)]. With this measurement, it is possible to deduce the contribution of the intact tunneling barrier. The dielectric breakdown of the barrier is confirmed via an additional TMR measurement after applying 3 V to the junction. During the breakdown, the resistance changes from the MΩ to the Ω range. After the breakdown, both the TMR and the TMS do not show any effect of magnetization switching [compare the inset of Fig. 4(a) to the minor loop shown in Fig. 1(b)].

Clearly, around 70% of the absolute thermovoltage is caused by the intact tunneling barrier in the case of small MTJ areas. This contribution decreases to 32% for larger MTJ areas. Since the laser has a spot size of 11 μm^2 when focused onto the MTJ [12], one possible explanation for the decrease is the occurrence of nonhomogenous heating. Thus, additional lateral heat flows emerge, effectively lowering the temperature difference across the barrier and, ultimately, the measured thermovoltage. The regime of homogenous heating is indicated by the gray shaded area in Fig. 4(a), which represents the laser spot size. In future experiments, intermediate MTJ sizes could offer a more detailed insight into the processes of nonhomogenous heating and in-plane temperature differences. With additional in-plane temperature differences, Nernst effects and additional magnetothermopower contributions become possible, which are not taken into account in the current TMS experiments.

Figure 4(b) sums up the absolute thermovoltages in dependence of the RA product. Here, a laser power of 150 mW is applied to MTJs with an area of 6π μm^2. In the case of MAO, a drop of about 20 μV in the absolute thermovoltage is measured for barrier thicknesses of 1.8 and 2.0 nm, which correspond to the samples that were prepared separately from the rest of the series. Since the RA products, the barrier heights and the

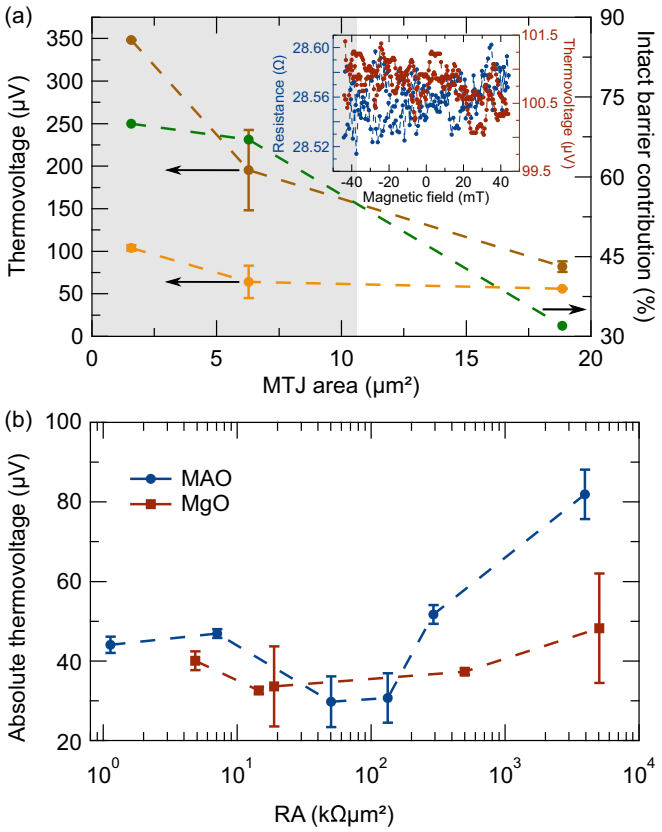

FIG. 4. (a) Absolute thermovoltage (dark orange) and thermovoltage after dielectric breakdown (light orange) depending on the MTJ area of the sample with a nominal barrier thickness of 2.6-nm MAO. The inset shows TMR and TMS measurements after applying 3 V to the junction and confirms the dielectric breakdown. Also, the contribution of the intact barrier to the absolute thermovoltage is shown (green) as well as the regime of homogenous heating (gray shaded area). (b) Measured absolute thermovoltages with a laser power of 150 mW of the MTJs with an area of 6π μm^2 depending on the RA product of all series.

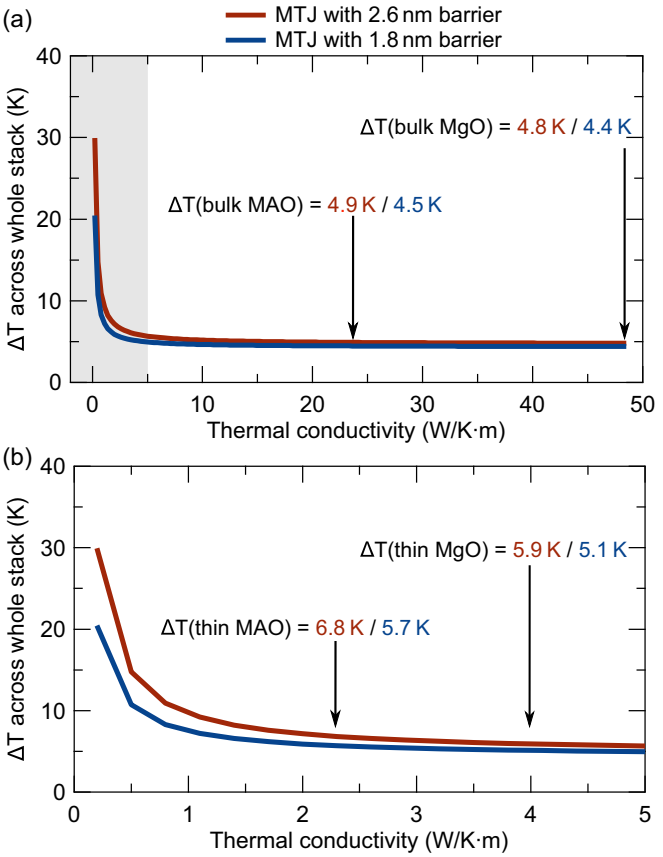

FIG. 5. (a) Dependence of the temperature difference across the whole stack on the thermal conductivity of the barrier including both bulk values of MAO and MgO for barrier thicknesses of 1.8 and 2.6 nm (laser power is 114 mW, deduced from calibration measurements). The thin-film regime is highlighted by the gray shaded area. (b) The thin-film regime with both MAO and MgO values for the two barrier thicknesses.

Brinkman barrier thicknesses of series I are in good agreement with each other, the only difference is the barrier asymmetry. All other MTJs with MAO barriers show a thermovoltage that is consistently larger by a factor of up to 2 in comparison with the MTJs with MgO barriers.

In general, an increasing barrier thickness results in an increased temperature difference and, ultimately, in an increased measured thermovoltage. The difference in the MTJs with MAO barrier thicknesses of 1.8 and 2.0 nm in comparison to the rest of the series is explainable by the addition of an automated sample stage controller. Reference [12] found that a difference in the z position of 1 μm can influence the measured thermovoltage by as much as 20% (indicated by the larger error bars of the samples with 1.8 and 2 nm of MAO). Martens *et al.* [12] also describe the automated sample stage in more detail. Excluding the two samples with MAO barriers, the difference between series I and series II is explainable by the different thermal conductivities of thin MAO and MgO films resulting in different temperature differences across the barrier and, thus, different thermovoltages.

Bulk MAO has a thermal conductivity of 23 W K^{-1} m^{-1} [36], whereas bulk MgO has a thermal conductivity of 48 W K^{-1} m^{-1} [37]. In Ref. [37] the thermal conductivity of thin MgO films also is determined experimentally to be 4 W K^{-1} m^{-1}. Taking the same reduction factor for thin MAO films, resulting in a thermal conductivity of 2.3 W K^{-1} m^{-1}, a COMSOL simulation offers insight into the actual temperature difference across the whole stack.

Figure 5(a) displays the result of this simulation for the interesting range of thermal conductivity and two barrier thicknesses. Accordingly, the thin-film regime is shown in Fig. 5(b). Since the area of the MTJs (1.6 μm^2) is smaller than the area of the focused laser beam (11 μm^2), the MTJs are heated homogeneously. The temperature differences become very large in comparison to the values of preceding publications [2] (here, the laser spot area was usually around 240 μm^2) since most of the laser-beam energy is absorbed directly above the MTJ instead of a larger area of the Au bond pad. A systematic study of the influence of the laser spot size can be found in Ref. [12]. Of course, with the lack of actual measurements of the thermal conductivity of thin insulating films, COMSOL simulations offer only limited insight into the

actual thermal distribution inside a MTJ. Hence, there is an ongoing discussion about the actual thermal conductivity of thin insulating films [13,15,38].

With the simulated temperature differences, the Seebeck coefficients for the MAO and the MgO MTJs with the highest TMS ratios are calculated (via $\mathrm{TMS} = \frac{S_p - S_{ap}}{\min(|S_p|, |S_{ap}|)}$) to be $S_p = -51$ and $S_{ap} = -56\ \mu\mathrm{V/K}$ for MAO and $S_p = -12$ and $S_{ap} = -15\ \mu\mathrm{V/K}$ for MgO, which is in good agreement with previous results [2,8–11].

IV. CONCLUSION

We have studied the dependence of the laser-induced TMS effect on the barrier thickness of MAO and MgO MTJs and found a distinct maximum of the TMS ratio in the case of thick barriers (nominal barrier thickness of 2.6 nm) for both materials. The TMS ratio increased from (3 to 4)% to 8% for MTJs with the MAO barriers, whereas the TMS ratio for MTJs with the MgO barrier increased from around 15% to 28%. We found no experimental evidence of enhanced interface effects, which could explain the predicted increase in the TMS effect in the case of thin barriers. The Brinkman model offered detailed insight into the barrier heights and asymmetries of the MTJs with MAO barriers. A changing barrier asymmetry did not influence the TMS ratio, and thus the asymmetry of the transmission function, which we attribute to the Brinkman barrier asymmetry being a geometric parameter, whereas the transmission function of the MTJ depends on the energy. In addition, the extracted Brinkman barrier thicknesses provided a convenient way to compare samples with different nominal barrier thicknesses.

Furthermore, we measured very high thermovoltages of more than 350 μV at the smallest MTJs of $0.5\pi\ \mu\mathrm{m}^2$ with a MAO barrier, in contrast to 90 μV for MTJs with barriers of MgO. This difference also is reflected in the dependence of the thermovoltage on the barrier thickness. Here, MAO barriers show a thermovoltage that is larger by a factor of 2 in comparison with MgO barriers. Additionally, the MTJ with the MAO barrier exhibits Seebeck coefficients that are three times as large as for MTJs with the MgO barriers ($S_{p,\mathrm{MAO}} = -59\ \mu\mathrm{V/K}$ versus $S_{p,\mathrm{MgO}} = -18\ \mu\mathrm{V/K}$) taking the reduced thermal conductivity of thin insulating films into account. A thorough investigation of the contribution of the remaining thermovoltage to the absolute thermovoltage after dielectrically breaking the barriers revealed a significant deviation in case of nonhomogenous heating. Although 70% of the absolute thermovoltages are attributed to the barrier of small MTJs, this contribution decreases to $\approx 30\%$ in the case of MTJ areas larger than the laser spot size. Thus, the effect of nonhomogenous heating and potential lateral heat flows needs to be addressed in future experiments. Overall, we conclude that MAO is generally preferable as a barrier material when generating thermovoltages in MTJs. Still, further effort is needed to determine the real thermal conductivities of thin insulating films.

ACKNOWLEDGMENTS

The authors gratefully acknowledge financial support from the Deutsche Forschungsgemeinschaft (DFG) within the priority program Spin Caloric Transport (SPP 1538, MU 1780/8-2, KU 3271/1-1, RE 1052/24-2, HE 5922/4-2, TH 1399/4-2).

[1] M. Czerner, M. Bachmann, and C. Heiliger, Phys. Rev. B **83**, 132405 (2011).
[2] M. Walter, J. Walowski, V. Zbarsky, M. Münzenberg, M. Schäfers, D. Ebke, G. Reiss, A. Thomas, P. Peretzki, M. Seibt, J. S. Moodera, M. Czerner, M. Bachmann, and C. Heiliger, Nat. Mater. **10**, 742 (2011).
[3] N. Liebing, S. Serrano-Guisan, K. Rott, G. Reiss, J. Langer, B. Ocker, and H. W. Schumacher, Phys. Rev. Lett. **107**, 177201 (2011).
[4] N. Liebing, S. Serrano-Guisan, K. Rott, G. Reiss, J. Langer, B. Ocker, and H. W. Schumacher, J. Appl. Phys. **111**, 07C520 (2012).
[5] N. Liebing, S. Serrano-Guisan, P. Krzysteczko, K. Rott, G. Reiss, J. Langer, B. Ocker, and H. W. Schumacher, Appl. Phys. Lett. **102**, 242413 (2013).
[6] N. Liebing, S. Serrano-Guisan, K. Rott, G. Reiss, and H. W. Schumacher, J. Magn. Magn. Mater. **400**, 154 (2016).
[7] J. Shan, F. K. Dejene, J. C. Leutenantsmeyer, J. Flipse, M. Münzenberg, and B. J. van Wees, Phys. Rev. B **92**, 020414(R) (2015).
[8] A. Boehnke, M. Milnikel, M. von der Ehe, C. Franz, V. Zbarsky, M. Czerner, K. Rott, A. Thomas, C. Heiliger, G. Reiss, and M. Münzenberg, Sci. Rep. **5**, 8945 (2015).
[9] A. Boehnke, U. Martens, C. Sterwerf, A. Niesen, T. Huebner, M. von der Ehe, M. Meinert, T. Kuschel, A. Thomas, C. Heiliger, M. Münzenberg, and G. Reiss, Nat. Commun. **8**, 1626 (2017).
[10] A. Boehnke, M. Walter, N. Roschwesky, T. Eggebrecht, V. Drewello, K. Rott, M. Münzenberg, A. Thomas, and G. Reiss, Rev. Sci. Instrum. **84**, 063905 (2013).
[11] T. Huebner, A. Boehnke, U. Martens, A. Thomas, J.-M. Schmalhorst, G. Reiss, M. Münzenberg, and T. Kuschel, Phys. Rev. B **93**, 224433 (2016).
[12] U. Martens, J. Walowski, T. Schumann, M. Mansurova, A. Boehnke, T. Huebner, G. Reiss, A. Thomas, and M. Münzenberg, J. Phys. D: Appl. Phys. **50**, 144003 (2017).
[13] T. Böhnert, R. Dutra, R. L. Sommer, E. Paz, S. Serrano-Guisan, R. Ferreira, and P. P. Freitas, Phys. Rev. B **95**, 104441 (2017).
[14] T. Böhnert, S. Serrano-Guisan, E. Paz, B. Lacoste, R. Ferreira, and P. P. Freitas, J. Phys.: Condens. Matter **29**, 185303 (2017).
[15] H. F. Yang, X. K. Hu, N. Liebing, T. Böhnert, J. D. Costa, M. Tarequzzaman, R. Ferreira, S. Sievers, M. Bieler, and H. W. Schumacher, Appl. Phys. Lett. **110**, 232403 (2017).
[16] C. Lopez-Monis, A. Matos-Abiague, and J. Fabian, Phys. Rev. B **89**, 054419 (2014).
[17] C. Lopez-Monis, A. Matos-Abiague, and J. Fabian, Phys. Rev. B **90**, 174426 (2014).

[18] G. E. Bauer, E. Saitoh, and B. J. van Wees, Nat. Mater. **11**, 391 (2012).
[19] W. F. Brinkman, R. C. Dynes, and J. M. Rowell, J. Appl. Phys. **41**, 1915 (1970).
[20] M. Czerner and C. Heiliger, J. Appl. Phys. **111**, 07C511 (2012).
[21] C. Heiliger, C. Franz, and M. Czerner, Phys. Rev. B **87**, 224412 (2013).
[22] M. Hatami, G. E. W. Bauer, Q. Zhang, and P. J. Kelly, Phys. Rev. Lett. **99**, 066603 (2007).
[23] H. Yu, S. Granville, D. P. Yu, and J.-P. Ansermet, Phys. Rev. Lett. **104**, 146601 (2010).
[24] E. Padron-Hernandez, A. Azevedo, and S. M. Rezende, Phys. Rev. Lett. **107**, 197203 (2011).
[25] J. C. Leutenantsmeyer, M. Walter, V. Zbarsky, M. Münzenberg, R. Gareev, K. Rott, A. Thomas, G. Reiss, P. Peretzki, H. Schuhmann, M. Seibt, M. Czerner, and C. Heiliger, SPIN **03**, 1350002 (2013).
[26] A. Pushp, T. Phung, C. Rettner, B. P. Hughes, S.-H. Yang, and S. S. P. Parkin, Proc. Natl. Acad. Sci. USA **112**, 6585 (2015).
[27] Y. Miura, S. Muramoto, K. Abe, and M. Shirai, Phys. Rev. B **86**, 024426 (2012).
[28] J. Zhang, X. G. Zhang, and X. F. Han, Appl. Phys. Lett. **100**, 222401 (2012).
[29] H. Sukegawa, H. Xiu, T. Ohkubo, T. Furubayashi, T. Niizeki, W. Wang, S. Kasai, S. Mitani, K. Inomata, and K. Hono, Appl. Phys. Lett. **96**, 212505 (2010).
[30] B. Tao, D. Li, H. Liu, H. Wei, J.-F. Feng, S. Wang, and X. Han, IEEE Trans. Magn. **50**, 4401004 (2014).
[31] T. Scheike, H. Sukegawa, K. Inomata, T. Ohkubo, K. Hono, and S. Mitani, Appl. Phys. Express **9**, 053004 (2016).
[32] H. Sukegawa, S. Mitani, T. Ohkubo, K. Inomata, and K. Hono, Appl. Phys. Lett. **103**, 142409 (2013).
[33] B. S. Tao, H. X. Yang, Y. L. Zuo, X. Devaux, G. Lengaigne, M. Hehn, D. Lacour, S. Andrieu, M. Chshiev, T. Hauet, F. Montaigne, S. Mangin, X. F. Han, and Y. Lu, Phys. Rev. Lett. **115**, 157204 (2015).
[34] T. Katayama and S. Yuasa, Appl. Phys. Lett. **89**, 112503 (2006).
[35] B. Geisler and P. Kratzer, Phys. Rev. B **92**, 144418 (2015).
[36] St. Burghartz and B. Schulz, J. Nucl. Mater. **212–215**, 1065 (1994).
[37] S.-M. Lee, D. G. Cahill, and T. H. Allen, Phys. Rev. B **52**, 253 (1995).
[38] J. Zhang, M. Bachman, M. Czerner, and C. Heiliger, Phys. Rev. Lett. **115**, 037203 (2015).